IMPACT OF ACTIVATION IN PROJECTION WELDING WITH CAPACITOR DISCHARGE USING MULTIPHYSICS SIMULATION AND A PROCESS-INTEGRATED TRANSITION RESISTANCE MEASUREMENT

J. KOAL*, M. BAUMGARTEN**, J. ZSCHETZSCHE*, U. FÜSSEL*

*Technische Universität Dresden, Institute of Manufacturing Science and Engineering, Chair of Joining Technology and Assembly, Dresden, Germany, ORCiD: 0000-0003-0763-552X
**Technische Universität Dresden, Institute of Manufacturing Science and Engineering, Chair of Joining Technology and Assembly, Dresden, Germany, ORCiD: 0000-0001-8486-1235

DOI 10.3217/978-3-85125-968-1-31

ABSTRACT

Capacitor discharge welding (CDW) is defined by a pulsed current profile. It is usually used for projection welding and is characterized by very high power density and very short welding time. The process can be classified into four phases: Contacting, Activating, Material Connection and Holding Pressure. High-speed images show the formation of metal vapor during the activation phase. This removes impurities and oxide layers from the contact zone and activates the surfaces. The material connection is achieved by pressing the activated surfaces together. The purpose of the investigation is to describe the impact of activation on the formation of the material connection.
A capacitor discharge welding system at the Technische Universität Dresden has the unique feature of interrupting the current flow at a given time. That allows different current profiles with the same rate of current increase. This unique feature permits the experimental investigation of activation and their impact on the formation of the material connection. To achieve this, projection components with different interruption times were welded. The transition voltages were measured before, while and after welding at each contact area. The mechanical strength of the welded joints was measured and a metallographic investigation was performed. To evaluate the impact of the activation in time and location, the experimental results were combined with simulative investigations. The evaluation of temperature and current density distributions enables the physical description of the activation. An iteratively coupled electrical-thermal and mechanical-thermal FEM-model was used. The experimental measured process variables force and current were used as boundary conditions for the simulation. A contact theory was implemented. In addition, the model considers temperature-dependent material characteristics and a remeshing procedure to model high projection deformations. The validation of the simulation was done by comparing measured and simulated transition voltages at the contact areas.

Keywords: Capacitor Discharge Welding, Projection Welding, Numerical Simulation, Contact Resistance, Transition Resistance, Activation

Symbol	Description	Unit
C	Capacity	F
E_{el}	Electrical energy	J
I	Current	A
j	Current density	A/m²
κ	Numerical parameter	-
ρ	Specific electric resistance	$\Omega \cdot \mathrm{m}$
ρ_1	Specific electric resistance of material 1	$\Omega \cdot \mathrm{m}$
ρ_2	Specific electric resistance of material 2	$\Omega \cdot \mathrm{m}$
ρ_{film}	Specific electric resistance of surface	$\Omega \cdot \mathrm{m}$
$\dot{q}$	Heat flux density	W/m²
Q	Amount of heat	J
$\dot{Q}$	Heat flux	W
$\dot{Q}_{\mathrm{W}}$	Heat flux caused by the resistance heating	W
$\dot{Q}_{\mathrm{R}}$	Heat flux caused by the contact resistance heating	W
R	Resistance	Ω
R_{K}	Contact resistance	Ω
σ_{s}	Yield strength of the soft material	N/mm²
σ_{K}	Contact pressure	N/mm²
t	Time	s
T	Temperature	T
U_{C}	Charging voltage	V
ξ	Numerical parameter	-

INTRODUCTION

Capacitor discharge welding (CDW or CD-Welding) is a stable, efficient, cost-effective and easy-to-use joining process. It is mostly used for projection welding. For example, finished components with diameters up to 200 mm can be welded in a few milliseconds [1]. The Chair of Joining Technology and Assembly at the Technische Universität Dresden has developed a new process understanding in recent years [2-4]. The process is classified into four phases transitioning into each other (contacting, activating, material connection, holding pressure). When activating, the power density in the joining zone is so high that metal vaporization appears. This results in the activation of the surfaces. The joint is established without a welding nugget. The joint is established just by pressing the activated surfaces together. Plastic deformation of the projection activates further surface areas by displacing the surface layer. Activation by metal vaporization has been verified by high-speed imaging [2, 3]. It has not been possible yet to determine the impact of activation, because the joint is formed under electrical, thermal and mechanical stress, hidden and nearly immediately within a very short time (5 to 15 ms). Only by numerical process simulation, it is possible to investigate the hidden short-time process in a location- and time-dependent way. The finite element method allows electrical, thermal and mechanical evaluation, local resolution of the stress, time resolution of the stress and sensitive analysis with boundary conditions that cannot be adjusted experimentally. Therefore, a numerical simulation model has been developed to provide a more holistic representation of the CD projection welding process. The joining process includes the following complexities that make model development difficult:

- Very high temperature gradients

- Strong temperature-dependent deformation of the projection
- Emergence of different phases (melt, metal vaporization)

The high temperature-dependent projection deformations produce a high distortion of the mesh. This results in convergence problems. To avoid this, the simulation model must be remeshed at the time of strong distortion [5-7]. By experimental investigations on a new machine technology for CD welding, it is possible to measure transition resistances before and after welding in a process-integrated way for the first time. The current flow can also be interrupted. This means that for the first time, different current intensities can be investigated at the same rates of current rise. In addition to the simulative analysis, this also enables an experimental estimation of the influence of activation.Capacitor Discharge projection Welding

PROCESS FUNDAMENTALS

CD welding is mostly used for projection welding and is a conductive resistance welding process. Before starting the welding process, one or more capacitor banks are charged. This causes an electrical energy E_{el} to be stored in the capacitor as a function of the charging voltage U_{C} and the capacity C (see equation 1) [8].

$$E_{\mathrm{el}} = \frac{1}{2} C * {U_C}^2 \tag{1}$$

Discharging the electrical energy E_{el} starts the welding process. The current flow is transferred to the joining point. This results in the transformed and unregulated welding current as shown in Fig. 1. The peak current I_{p} is reached in a few milliseconds. This time is called the current rise time t_{p}. The welding time t_{h} is reached when the peak current I_{p} drops by 50 %. The current flow time t_{l} is reached when the current drops to 95 %. [1]

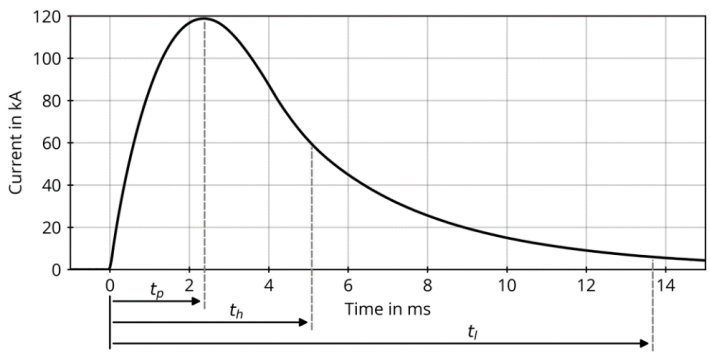

Fig. 1 Characteristic current curve of a capacitor discharge projection welding

This clearly illustrates the differences to mid-frequency (MFDC) spot welding. This means that very high current intensities are obtained in very short current rise times [1, 9]. The projection geometry in the joining zone focuses the current flow and therefore increases the electric current density j. Based on Joule's heat law, the amount of heat Q is

generated in an electrical wire as a function of the square of the current and the ohmic resistance R (see equation 2). A differential observation based on equation 3 allows the local description of the heating by the heat flux density $\dot{q}$. This depends on the specific electric resistance ρ of the material and the current density j. The differential description is useful, for example, for using the finite element method (FEM). Equation 3 shows that a high current density in the joining zone results in a high heat flux density. The high power density in the joining zone is the critical parameter for the heating of the short-time projection welding process. That's why the heat flux $\dot{Q_{\mathrm{W}}}$ caused by the resistance heating in the projection and component is much smaller than the heat flux $\dot{Q_{\mathrm{R}}}$ caused by the contact resistance heating in the joining zone at the beginning of the process (see equation 4). As a result, no weld lenses are obtained in CD projection welding (see Fig. 2). [10]

$$Q = I^2 \cdot R \cdot t \tag{2}$$

$$\dot{q} = \frac{\dot{Q}}{V} = \rho \cdot j^2 \tag{3}$$

$$\dot{Q_{\mathrm{R}}} = \iint j^2 \cdot R_{\mathrm{C}} \cdot dA \gg \dot{Q_W} = \iiint I^2 \cdot R \cdot dV \tag{4}$$

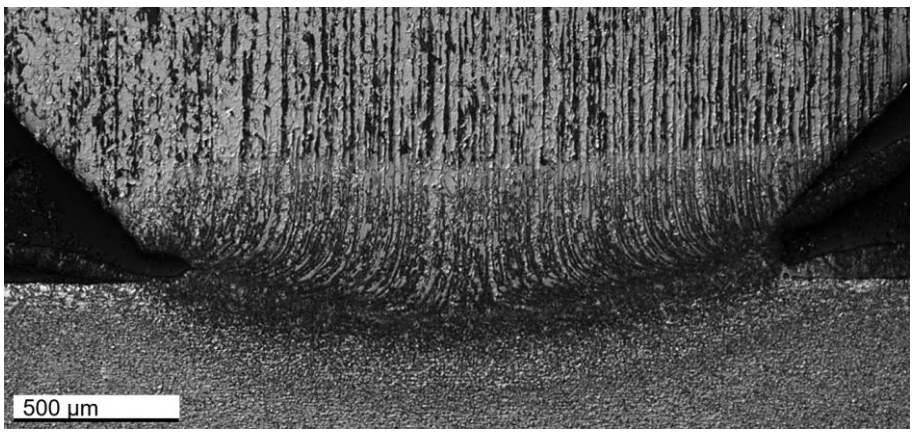

Fig. 2 Missing of a joint without nugget lens in the joining zone during CD projection welding

SURFACE ACTIVATION

Investigations using high-speed imaging have shown that metal vaporization occurs due to the high power density in the joining zone [10]. CD projection welding is always associated with the appearance of weld spatter. Objective criteria for evaluating weld spatter were defined in [10]. This makes it possible to classify the weld spatter into four classes (classes 0 to 3). These classes are shown in Fig. 3. No sparks or weld spatter can be detected in class 0. Only a glow in the contact area may be visible. There is hardly any weld spatter visible in Class 1. These glow after a very short time. In Class 2, weld spatter

is clearly visible. The direction of travel of the weld spatter is towards the ground. They do not reach the ground. Strong weld spatter can be seen in Class 3, which flies down to the ground and can also continue to glow there.

In [2-4] a new process understanding with four characteristic phases has been defined: Contacting, Activating, Material Connection and Holding Pressure. When contacting the electrodes moves onto the components. The electrode force is increasing up to the predefined welding force. Plastic deformation begins in the contact area of the projection. When activating, the current flow starts with high current density gradients. This results in very high power densities in the contact area. This eliminates the foreign and oxide layers on the surfaces. With this begins the activation of the contact surface. To build the material connection, the activated contact areas are pressed together. The current and the current density decreases. The heat conduction of the projection starts. Further softening and plastic deformation of the projection occurs. With a further decrease of the current density, the last phase begins: Holding Pressure. The electrodes continue to follow-up. Further plastic deformation of the projection continues. This increases the contact area. Finally, the follow-up of the electrodes ends. The heat conduction continues and the joining zone is cooling down.

Following the characterization of the process phases, an activation of the surface by metal vaporization is necessary for the formation of the material connection. This means that a joint cannot be formed without activation. A capacitor discharge welding system at Technische Universität Dresden has the unique property of interrupting the current flow at a specific point of time. This allows different current profiles at the same rate of current rise. This unique feature allows the experimental investigation of activations and their effects on the formation of the material connection.

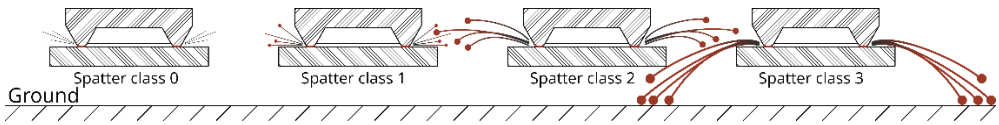

Fig. 3 Classification of welding spatters in capacitor discharge welding [9]

NUMERICAL SIMULATION

In addition to the experimental investigation of surface activation, the finite element method can also be used. The FEM allows an electrical, thermal and mechanical evaluation, local resolution of the stress, temporal resolution of the stress and sensitive analyses with boundary conditions that cannot be set experimentally. An iteratively coupled simulation model for CD projection welding was developed at the Technische Universität Dresden with *ANSYS MECHANICAL APDL*. The iterative simulation process is described in detail in [11]. Input data are the current and the force as a function of time by experimental measurement data. The mechanical environment is solved for a small time step Δt. Then the contact pressure σ_K is determined in all contact areas. Using the contact pressure σ_{K} and the room temperature T_R at the beginning, it is possible to calculate the contact resistance R_{C} by equation 5 [12]. This temperature and contact

pressure dependant contact theory according to SONG is validated for projection welding of steel alloys. The yield strength σ_s of the soft material, the specific electric resistances $\rho_{1,2}$ and a specific film resistance ρ_{film} are considered. Two numerical parameters are also considered. According to Song, the numerical parameters ξ and κ describes the surface condition.

$$R_K(T, \sigma_K) = 3\xi \cdot \left(\frac{\sigma_s(T)}{\sigma_K \kappa}\right) \cdot \left(\frac{\rho_1(T)+\rho_2(T)}{2} + \rho_{\text{film}}\right) \quad (5)$$

The developed numerical process simulation is adapted to experimental measurement data. For this, the transition voltages $U_{e,p}$, $U_{p,s}$ und $U_{s,e}$ of the single contact zones are measured during the process. When evaluating the transition voltages, they are corrected by subtracting the induced voltage of the CD welding machine [13]. The measurement setup is shown in Fig. 4a. The numerical parameters are time varied in the numerical process simulation so that the voltage curve matches the reality (Fig. 4b). [11]

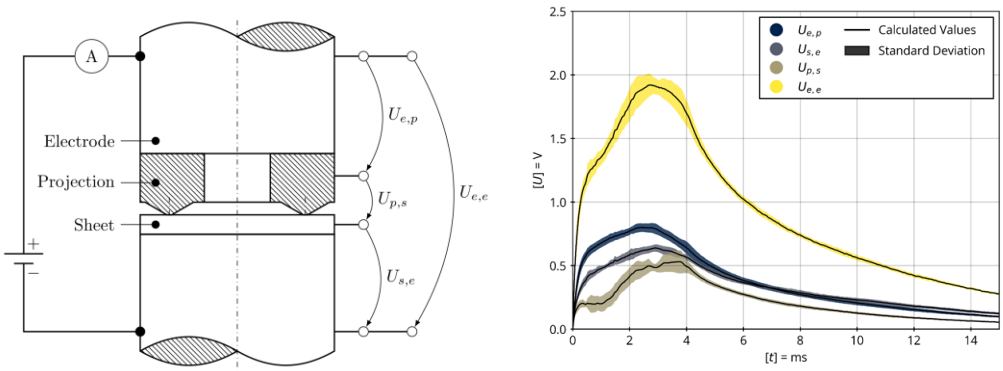

a) Experimental Setup

b) Voltage curve of all contact zone

Fig. 4 Experimental Setup to measure the dynamic transition resistance for adjusting the numerical parameters for all contact zones

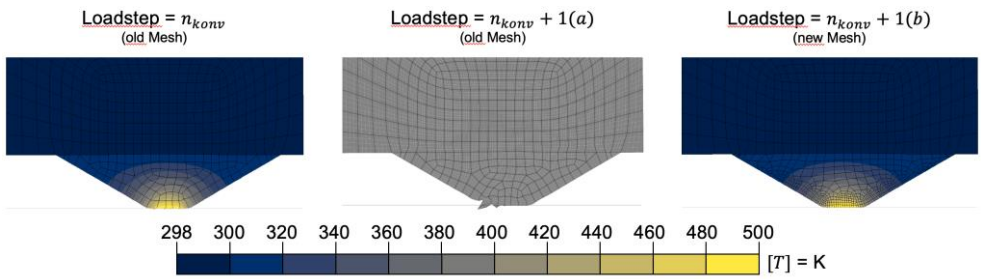

Fig. 5 Illustration of the remeshing process within a structure simulation. A deformation of the projection is calculated for the given temperature distribution. From left to right: last converged load step (n_{konv}), convergence problems in the following load step (n_{konv} + 1 (a)), converged solution after remeshing (n_{konv} + 1 (b))

With the progress of the simulation time, strong temperature-dependent plastic deformation appears. These result in such strong mesh distortions that convergence problems occur. Therefore, a remeshing is necessary [5-7]. Fig. 5 shows a situation where mesh distortion becomes too big. The initial situation for the remeshing process is a converged solution n_{konv}. The next load step $n_{\mathrm{konv}} + 1(a)$ results in convergence problems because of strong mesh distortion. A remeshing will result in the solution of the load step $n_{\mathrm{konv}} + 1(b)$.

Since the distortion of the mesh with the high temperature-dependent deformation occurs in the mechanical environment, remeshing starts there. Proprietary simulation applications usually provide remeshing for structural analysis to calculate large deformations [14]. In the thermo-electric environment, these tools usually cannot be used. Therefore, the challenge is to remesh the thermo-electric environment as well and implement it into the iteratively coupled simulation process. Both indirectly coupled simulation environments require the same mesh. To do this, the last converged load step in the structural simulation is loaded. The global node coordinates (physical coordinates) are exported. The remeshing is then performed in the region of greatest distortion. Based on the new mesh geometry, the thermo-electric simulation must be continued. For this, the temperature distribution on the old mesh must be transferred to the new mesh generated in the mechanical domain. To do this, all the associated elements of new coordinates are defined in the old mesh. Then the natural node coordinates (element coordinates from -1 to 1) of the new physical coordinates in the old elements are determined. With the determined natural node coordinates, the temperature and electric voltage can be interpolated using to the element solution of the old mesh and the shape functions. At the end, interpolated solutions are available for all nodes in the new mesh, which can be applied as initial conditions. As a last step, a converged solution on the new mesh must be generated in order to continue the thermal electric simulation.

EXPERIMENTAL AND NUMERICAL PROCEDURE AND RESULTS

EXPERIMENTAL INVESTIGATION

The resistance welding task consists of a sheet and a ring projection with a projection diameter d_{R} = 15 mm, radial contact area A_R = 1 mm and a projection angle α_{R} = 45° (see Fig. 6a). The sheet thickness of the component is t_{s} = 3 mm. The ring projection and the sheet are made of S355MC. The resistance welding electrodes are made of CuCr1Zr. The investigations are performed on a portal system „*KKP 18-MCS/gKE*“ of the company Kapkon GmbH. The system has an electric servo motor with an electrode force of up to 30 kN. It is possible to weld both MFDC and CD. This enables investigation of the electrical influence on the welded joint without affecting the mechanics. Four capacitor banks are available for capacitor discharge. Peak currents of up to 210kA in 2.1ms can be realized. A unique feature is the process-integrated transition resistance measurement during CD welding. During the transition resistance measurement, the CD circuit is disconnected so that the measurement current flows solely through the welding task. Additionally, current flows in the welding process can be interrupted using a pulsed

capacitor discharge. This results in different current profiles depending on the interruption time t_I. Fig. 6b shows this behavior. The capacitor bank was charged with a voltage U_C = 1000 V. This capacitor bank has a capacity of 21320 µF. This charging voltage U_C allows the activation to be investigated, since no welding connection is established at an interruption time t_I = 0.4 ms and the upper limit of the welding range has been established at an interruption time t_I = 30 ms. The interruption time t_I = 30 ms is equivalent to no interruption, because after 30 ms the capacitor banks are already completely discharged. The upper limit is defined by the appearance of class 2 to 3 weld spatter and by imperfections in the cross section. A total of 11 interruption times t_I were investigated. Each interruption time was repeated 7 times. A static press-out test was performed for each experiment. A total of 76 experiments were evaluated, as one false measurement was removed.

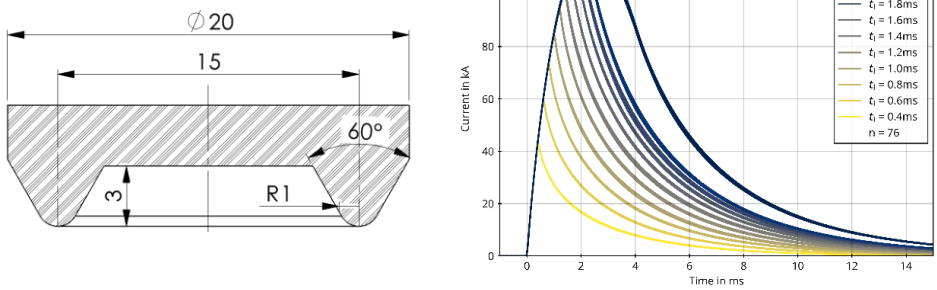

a) Geometry of investigated projection b) Current curves at interruption time t_I

Fig. 6 Geometry of the ring projection and current curves as a function of the interruption time t_I

The results of the transition resistance measurement before and after welding are shown in Fig. 7a. An instantaneous drop of all transition resistances R_T can be observed at an interruption time of t_I = 0.4 ms. The drop in the transition resistances R_T changes the order of the single transition resistances R_{EP}, R_{PS}, R_{SE}. The transition resistance R_{EP} in the welding zone now represents the largest value of 14.35 µΩ ± 0.03 µΩ for t_I = 0.4 ms. The transition resistance before welding was R_{PS} 35.27 µΩ ± 0.16 µΩ. At an interruption time of t_I = 0.4 ms no material connection is established, even though the resistances drop significantly. Only at an interruption time of t_I = 0.8 ms and bigger it is possible to establish a material connection. The transition resistances have fallen further to R_{PS} 10.66 µΩ ± 0.02 µΩ. But that does not mean high press-out forces F_Z = 6.87 kN ± 1.06 kN (see Fig. 8) can be reached. Fig. 7b shows a detailed evaluation of the transition resistances after welding. Especially in the joining zone, the transition resistance R_{EP} decreases strongly with an increase of the interruption time from t_I = 0.4 ms to t_I = 0.6 ms (-4.08 µΩ ≙ 28.4 %). As the process continues, the transition resistances continue to decrease. From an interruption time t_I = 1.4 ms a value of approx. 7.3 µΩ until 7.8 µΩ is reached for the joining zone. From this time on, the destructive force F_Z of the press-out

test also stops increasing and varies between 23 kN until 30 kN (see Fig. 8). A connection is completely established at an interruption time of t_I = 1.4 ms and more. The further energy up to t_I = 30 ms does not provide a significant increase of the press-out force. Only from t_I = 30 ms a lower standard deviation is evident. But in this range, a spatter class 3 is always detected or bonding defects are present in the microsection.

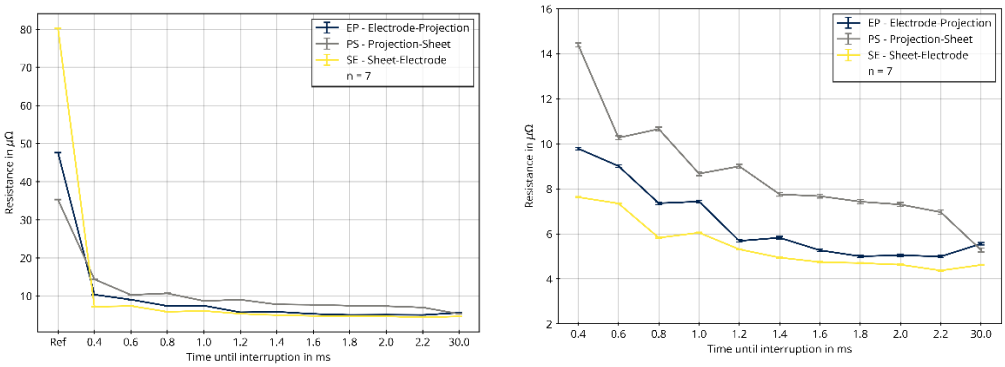

a) R_T before (REF) and after welding

b) Detail view of R_T after welding

Fig. 7 Transition resistances R_T before and after welding. Before welding is the reference (REF)

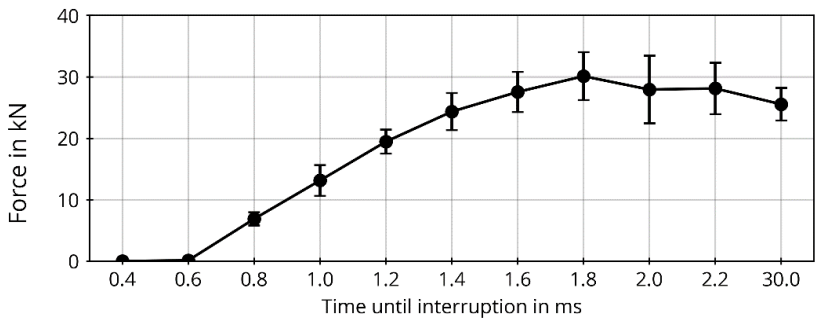

Fig. 8 Press-out force F_Z of the ring projections as a function of the interruption time t_I

NUMERICAL INVESTIGATION

The numerical process simulation is based on the modeling method according to [11]. This considers the continuous adjustment of the contact resistance as a function of temperature and contact pressure, a nonlinear adaptive remeshing according to [7], the input parameters as time-dependent measurement data and the temperature-dependent material data for S355MC and CuCr1Zr. The material data used are in the appendix. In

Table 1 are the temperature-dependent thermomechanical properties of S355MC. In Table 2 are the temperature-dependent thermomechanical properties of CuCr1Zr. Table 4 and Table 5 show the corresponding temperature-dependent flow-stress curves for S355MC. In [15] the flow-stress curves for CuCr1Zr are shown.

The experimental investigations have shown that a significant collapse of the transition resistances already begins at t_I = 0.4 ms. Fig. 9a shows the temperature distribution for the time t = 0.4 ms. The heating is the highest at the edges of the projection cross-section. The temperature is about 80 K over the value in the middle of the cross section. Fig. 9b shows the temperature distribution for t = 0.8 ms. A connection might be established at this time. The heating continues to increase at the edge of the projection cross-section, since the contact resistance heating continues to dominate over the conductive heating (see equation 4). The temperature difference is now about 220 K. No strong projection deformations are noticeable at both time points. The current density is at its highest in the regions of the highest temperature increases. The maximum current density at t = 0.4 ms is $j = 6.17 * 10^9$ A/m^2 and at t = 0.8 ms it is $9.07 * 10^9$ A/m^2. This results in a maximum power density of 0.585 MW/cm^2 at t = 0.4 ms and 1.501 MW/cm^2 at t = 0.8 ms.

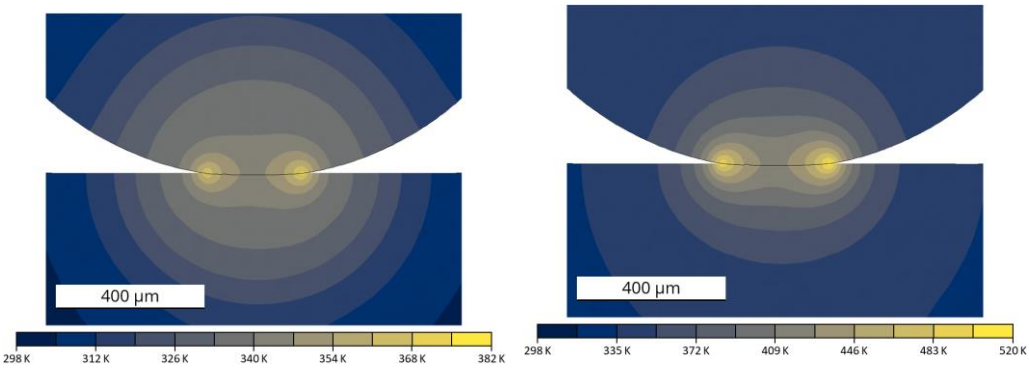

a) Temperature distribution at t = 0.4 ms b) Temperature distribution after t = 0.8 ms

Fig. 9 Temperature distribution of the numerical process simulation in the projection cross-section in the joining zone after different interruption times t_I

Fig. 10 shows the distribution of the current density j at the time of maximum current (I_w= 117 kA, t_w= 2.4 ms). This results in a maximum power density of 32.56 MW/cm^2. The deformation of the projection starts to increase further at this time. Contact resistance heating continues to be highest in the outer zone of the projection (T_{max} = 2100 K).

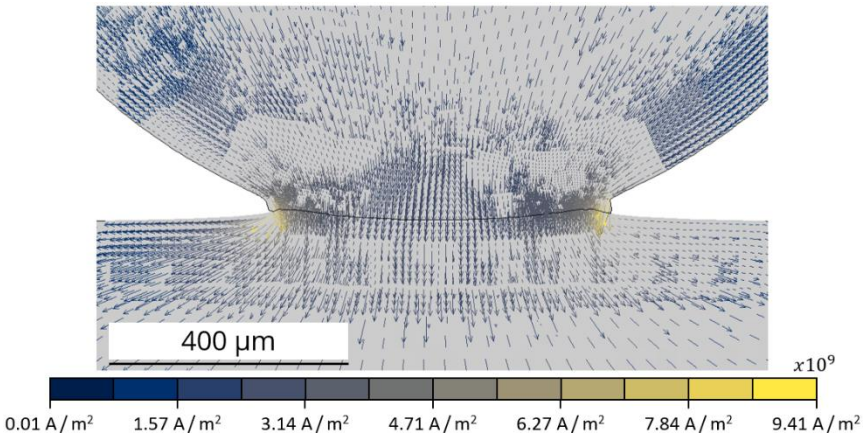

Fig. 10 Current density distribution at the time of maximum current (t = 2.37ms)

DISCUSSION

The decrease of the transition resistance in the contact zone points to a surface activation even at very low current maxima. With a small increase of the interruption time to t_I = 0.6 ms no connection could be established. It can be concluded that activation is not completed yet. With a further increase of to t_I = 0.8 ms a connection with low press-out forces can be reached. This shows that the surface activation at this point is enough to establish a connection. The remaining energy at this interruption time is not high enough to optimize the connection. As interruption times continue to increase, the connection quality becomes better. These investigations are consistent also with the observations from high-speed imaging [3, 10].

The numerical process simulation shows the heating in the outer area of the projection. This is the reason why the activation is clearly visible on the high-speed images. The heating proceeds from the outside to the inside. Investigations in laser keyhole welding with steel alloys indicate this. In laser keyhole welding a metal vapor-filled keyhole is formed, when high power densities are achieved. The required power densities depends on the material, the traveling speed and the depth of the keyhole. Recent investigations show that these vary between 1 and 5 MW/cm^2 [16-18]. The evaluation of the power density confirms the hypothesis of surface activation by metal vapor. These values are not reached with interruption times of t_I = 0.4 ms. The connection is also not established at these interruption times. However, the necessary power densities are reached at t_I = 0.8 ms and the formation of a welded connection can also be discovered for the first time. The power density in the joining zone increases with a further increase in the current intensity. The experiments also show this, because the splash class increases up to class 3. This defines the upper limit the welding range. The use of a multi-pulse technology is useful to further increase the connection quality. One pulse can be initiated to activate the surfaces. The connection is then established with a following second pulse.

The combination of experiment and simulation confirms the hypothesis of surface activation by metal vaporization. The formation of the connection by pressing activated

surfaces onto each other is to be analyzed in further investigations. Additionally, the activation of the surface is to be investigated as a function of different surface properties. Finally, further investigations with multi-pulse discharges are intended.

CONCLUSIONS

The experimental investigations show an immediate drop in the transition resistances of all contact zones after just $t_I = 0.4\,\text{ms}$. First connections could only be established after $t_I = 0.8\,\text{ms}$. The connection quality did not increase further after approximately $t_I = 1.4\,\text{ms}$. From the experimental investigations it can be concluded that activation does not occur sufficiently at the lowest interruption times. The temperature distribution and current density distribution were investigated in numerical simulations to describe this physically. It was determined that the heating occurs in the outer region of the projection and moves inward. The current density is also the highest there because of the concentration of heating in the outer region. Power density of $0.585\ \text{MW}/\text{cm}^2$ was observed for the interruption time $t_I = 0.4\,\text{ms}$. This is close to the power densities necessary for deep-hole welding. Metal vaporization is well known to occur there. Power densities of $1.501\ \text{MW}/\text{cm}^2$ are determined from an interruption time of $t_I = 0.8\,\text{ms}$ onwards. The occurrence of metal vaporization during CD projection welding for steel alloys can be demonstrated by combining experimental and simulative investigations. This also confirms the observations from high-speed imaging.

APPENDICES

Table 1 Thermophysical properties of S355MC

T / K	ρ_D / kg*m^{-3}	E / GPa	μ / 1	α / K^{-1}*10^{-5}	λ / W*m^{-1}*K^{-1}	h_V / MJ*m^{-3}	ρ / µΩ*mm^2*m^{-1}
298	7807	208	0.290	Reference	37.368	1	0.251
333	7797	207	0.291	3.185	38.113	10	0.272
373	7785	205	0.293	3.216	38.787	103	0.297
403	7775	204	0.294	3.239	39.163	216	0.317
433	7766	202	0.295	3.263	39.426	332	0.337
473	7753	199	0.297	3.296	39.601	491	0.366
503	7743	197	0.298	3.320	39.602	613	0.389
533	7733	195	0.299	3.345	39.497	737	0.413
573	7720	191	0.301	3.379	39.200	908	0.448
603	7710	189	0.302	3.405	38.871	1040	0.475
633	7700	186	0.303	3.432	38.458	1175	0.504
673	7686	181	0.304	3.468	37.799	1360	0.546
703	7675	178	0.306	3.495	37.236	1504	0.580
733	7664	175	0.307	3.523	36.627	1652	0.615
773	7650	170	0.308	3.561	35.768	1856	0.665
803	7639	166	0.309	3.590	35.102	2016	0.704

833	7628	162	0.311	3.619	34.433	2181	0.745
873	7612	156	0.312	3.659	33.550	2413	0.802
533	7733	195	0.299	3.345	39.497	737	0.413
573	7720	191	0.301	3.379	39.200	908	0.448
603	7710	189	0.302	3.405	38.871	1040	0.475
633	7700	186	0.303	3.432	38.458	1175	0.504
673	7686	181	0.304	3.468	37.799	1360	0.546
703	7675	178	0.306	3.495	37.236	1504	0.580
733	7664	175	0.307	3.523	36.627	1652	0.615
773	7650	170	0.308	3.561	35.768	1856	0.665
803	7639	166	0.309	3.590	35.102	2016	0.704
833	7628	162	0.311	3.619	34.433	2181	0.745
873	7612	156	0.312	3.659	33.550	2413	0.802
903	7602	152	0.314	3.691	32.478	2645	0.860
933	7593	147	0.316	3.725	31.742	2849	0.906
973	7581	141	0.318	3.774	30.823	3136	0.967
1003	7574	-	-	3.813	30.146	3368	1.011
1033	7577	-	-	3.868	29.055	3620	1.057
1073	7597	125	0.334	3.969	27.325	3956	1.103
1103	7605	-	-	4.039	26.694	4162	1.116
1133	7589	-	-	4.072	27.035	4291	1.126
1173	7566	-	-	4.116	27.512	4415	1.138
1203	7548	-	-	4.150	27.869	4546	1.147
1233	7531	-	-	4.184	28.227	4678	1.156
1273	7508	105	0.351	4.232	28.703	4855	1.167
1303	7491	-	-	4.269	29.060	4987	1.176
1343	7469	-	-	4.320	29.535	5165	1.187
1373	7451	-	-	4.360	29.891	5300	1.195
1403	7434	-	-	4.401	30.246	5435	1.202
1433	7417	-	-	4.443	30.601	5571	1.210
1473	7394	84	0.363	4.501	31.076	5751	1.220
1503	7378	84	0.363	4.546	31.434	5885	1.227
1533	7362	84	0.363	4.593	31.791	6019	1.234
1573	7341	84	0.363	4.658	32.269	6198	1.243
1603	7325	84	0.363	4.708	32.627	6333	1.250
1633	7309	84	0.363	4.761	32.984	6469	1.256
1673	7287	84	0.363	4.833	33.461	6651	1.264
1703	7271	84	0.363	4.889	33.819	6788	1.271
1733	7250	84	0.363	4.937	34.144	6946	1.291
1738	7192	84	0.363	4.824	33.917	7203	1.369
1743	7165	84	0.363	4.777	33.843	7350	1.409
1748	7153	84	0.363	4.764	33.851	7427	1.406
1753	7139	84	0.363	4.745	33.844	7518	1.403
1758	7121	84	0.363	4.718	33.819	7627	1.399
1763	7099	84	0.363	4.679	33.767	7760	1.394
1768	7071	84	0.363	4.625	33.679	7930	1.388

1773	7034	84	0.363	4.548	33.538	8149	1.380
1778	6983	84	0.363	4.436	33.318	8445	1.371
1803	6924	84	0.363	4.357	33.519	8789	1.367
1833	6900	84	0.363	4.382	34.067	8929	1.372
1873	6868	84	0.363	4.416	34.798	9114	1.379
1973	6785	84	0.363	4.500	36.626	9566	1.396
2073	6700	84	0.363	4.585	38.454	10000	1.414
2173	6613	84	0.363	-	40.282	10420	1.431
2273	6525	84	0.363	4.754	42.109	10820	1.448
2373	6435	84	0.363	-	43.937	11200	1.465
2473	6344	84	0.363	-	45.765	11570	1.482
2573	6251	84	0.363	-	47.593	11920	1.499
2673	6158	84	0.363	-	49.420	12250	1.516
2773	6065	84	0.363	5.176	51.248	12560	1.532
2873	5971	84	0.363	-	53.076	12860	1.549
2973	5877	84	0.363	-	54.904	13150	1.566
3073	5782	84	0.363	-	56.732	13420	1.583
3173	5688	84	0.363	-	58.559	13670	1.600
3273	5594	84	0.363	-	60.387	13900	1.616

Table 2 Thermophysical properties of CuCr1Zr

T / K	ρ_D / kg*m^{-3}	E / GPa	μ / 1	α / K^{-1}*10^{-5}	λ / W*m^{-1}*K^{-1}	h_V / MJ*m^{-3}	ρ / μΩ*mm^2*m^{-1}
298	8882	87.8	0.326	Reference	326	0	0.021
473	8803	81.0	0.298	1.650	305	623	0.033
573	8755	-	-	1.720	291	968	0.039
673	-	77.9	0.279	-	-	-	-
773	8656	-	-	1.800	281	1660	0.054
873	-	69.6	0.230	-	-	-	-
973	8549	-	-	1.890	275	2820	0.070
1073	-	65.1	0.238	-	-	-	-
1173	8425	60.6	0.212	2.020	268	3680	0.098

Table 3 Flow-stress curve of S355MC for 298 K until 673 K

	σ_F / MPA							
ϵ / 1	298 K	323 K	373 K	423 K	473 K	523 K	573 K	673 K
0.00	277.2	252.6	217.5	193.8	177.0	164.7	155.4	142.8
0.02	422.3	393.1	350.3	320.5	298.4	281.3	267.4	245.7
0.04	466.8	435.6	389.6	357.4	333.4	314.6	299.2	274.6
0.06	495.6	463.0	415.0	381.3	356.1	336.2	319.8	293.4
0.08	517.2	483.7	434.2	399.3	373.2	352.5	335.3	307.5
0.10	534.7	500.4	449.7	413.9	387.0	365.7	347.9	319.0
0.15	568.2	532.4	479.4	441.9	413.6	391.0	372.1	340.9
0.20	593.3	556.4	501.8	463.0	433.6	410.1	390.4	357.4
0.25	613.6	575.8	519.8	480.0	449.8	425.6	405.1	370.8
0.30	630.7	592.2	535.1	494.4	463.5	438.6	417.6	382.1
0.35	645.5	606.4	548.3	507.0	475.4	450.0	428.5	392.0
0.40	658.6	619.0	560.1	518.1	486.0	460.1	438.1	400.7
0.50	681.2	640.6	580.3	537.2	504.2	477.5	454.7	415.7
0.60	700.2	658.9	597.3	553.3	519.6	492.2	468.7	428.5

0.70	716.7	674.7	612.1	567.3	532.9	504.9	480.9	439.5
0.80	731.3	688.7	625.3	579.8	544.8	516.3	491.7	449.3
0.90	744.5	701.4	637.1	591.0	555.5	526.5	501.5	458.1
1.00	756.4	712.8	647.9	601.2	565.2	535.8	510.4	466.2
2.00	840.1	793.3	723.4	672.9	633.7	601.3	573.0	522.7

Table 4 Flow-stress curve of S355MC from 773K until 1673K

	σ_F / MPA						
ϵ / 1	773 K	873 K	973 K	1073 K	1273K	1473K	1673K
0.00	135.5	135.4	131.9	0.0	58.4	42.3	34.8
0.02	228.7	214.3	200.9	0.0	101.2	72.5	41.4
0.04	254.9	237.4	221.8	0.0	116.2	83.1	41.4
0.06	271.7	252.3	235.2	0.0	126.1	83.1	41.4
0.08	284.4	263.4	245.3	0.0	133.7	83.1	41.4
0.10	294.7	272.4	253.4	0.0	139.9	83.1	41.4
0.15	314.3	289.7	269.0	0.0	151.9	83.1	41.4
0.20	329.1	302.6	280.7	0.0	161.1	83.1	41.4
0.25	341.0	313.0	290.1	0.0	167.5	83.1	41.4
0.30	351.1	321.8	298.1	0.0	167.5	83.1	41.4
0.35	359.9	329.4	305.0	0.0	167.5	83.1	41.4
0.40	367.7	336.1	311.1	0.0	167.5	83.1	41.4
0.50	381.0	347.7	321.6	0.0	167.5	83.1	41.4
0.60	392.3	357.5	330.4	0.0	167.5	83.1	41.4
0.70	402.1	366.0	338.1	0.0	167.5	83.1	41.4
0.80	410.8	373.5	344.9	0.0	167.5	83.1	41.4
0.90	418.7	380.2	346.3	0.0	167.5	83.1	41.4
1.00	425.8	386.4	346.3	0.0	167.5	83.1	41.4
2.00	475.8	429.4	346.3	0.0	167.5	83.1	41.4

References

[1] DEUTSCHER VERBAND FÜR SCHWEIßEN UND VERWANDTE VERFAHREN E.V.: *Kondensatorentladungsschweißen – Grundlagen, Verfahren und Technik*, DVS Merkblatt 2911, Düsseldorf, 2016.

[2] U. FÜSSEL, M.-M. KETZEL, J. ZSCHETZSCHE: 'Erwärmungsverhalten der Kontaktzone beim Kondensatorentladungsschweißen unter Berücksichtigung der dynamischen Stromänderung und des Nachsetzverhaltens der Elektroden', *Abschlussbericht IGF- Nr. 18.987 BR/DVS-Nr. 04.069*, Technische Universität Dresden, Dresden, 2018.

[3] J. ZSCHETZSCHE, M.-M. KETZEL, U. FÜSSEL, H.-J. RUSCH, N. STOCKS: 'Process Monitoring at Capacitor Discharge Welding', *ASNT Research Symposium 2019, Proceedings*, 2019.

[4] N. STOCKS: *Erhöhung der Verschleißbeständigkeit durch partielle Integration von Hartmetallinserts mithilfe der KE-Mehrpulstechnik*, Ph.D Thesis, Technische Universität Dresden, Institute of Manufacturing Science and Engineering, Dresden, 2021.

[5] M. WEHLE: *Basics of Process Physics and Joint Formation in Resistance Projection Welding Processes*, Ph.D Thesis, University of Stuttgart, Institute of Materials Science, Stuttgart, 2020.

[6] F. X. LONG: *Development of a Remeshing Method for the Finite-Element Simulation of a Capacitor Discharge Press Fit Welding Process*, Bachelor Thesis, Karlsruhe Institute of Technology, Karlsruhe, 2018.

[7] J. KOAL, M. BAUMGARTEN, J. ZSCHETZSCHE, U. FÜSSEL: *Numerische Simulation großer Deformationen beim Buckelschweißen durch Kondensatorentladung*, DVS Congress 2021, Essen, 2021.

[8] H. BUMILLER, M. BURGMAIER, W. EICHLER, B. FEUSTEL, T. KÄPPEL, W. KLEE, J. MANDERLA, O. REICHMANN, J. SCHWARZ, K. TKOTZ, U. WINTER, K. ZIEGLER: *Electrical Engineering Textbook*, Europa Lehrmittel, ISBN: 3808532408, 2016.
[9] U. DILTHEY: *Schweißtechnische Fertigungsverfahren*, 1. Springer-Verlag GmbH, ISBN: 9783540331544, 2006.
[10] M.-M. KETZEL, M. HERTEL, J. ZSCHETZSCHE, U. FÜSSEL: 'Heat development of the contact area during capacitor discharge welding', *Welding in the World*, Vol. 63, No. 5, pp. 1195-1203, 2019.
[11] J. KOAL, M. BAUMGARTEN, S. HEILMANN, J. ZSCHETZSCHE, U. FÜSSEL: 'Performing an Indirect Coupled Numerical Simulation for Capacitor Discharge Welding of Aluminium Components', *Processes*, Vol. 8, No. 11: 1330, 2020.
[12] Q. SONG: *Testing and Modeling of Contact Problems in Resistance Welding*, Ph.D Thesis, Technical University of Denmark, Kongens Lyngby, Denmark, 2003.
[13] M.-M. KETZEL, J. ZSCHETZSCHE, U. FÜSSEL: 'Elimination of voltage measuring errors as a consequence of high variable currents in resistance welding', *Welding and Cutting*, Vol. 16, No. 3, pp. 164-168, 2017.
[14] ANSYS INC.: *Documentation Mechanical APDL – Chapter 4: Rezoning*, 2022.
[15] J. WANG, H. P. WANG, F. LU, B. E. CARLSON and D. R. SIGLER: 'Analysis of Al-steel resistance spot welding process by developing a fully coupled multi-physics simulation model', *International Journal of Heat and Mass Transfer*, Vol. 89, pp. 1061-1072, 2015.
[16] V. SEMAK, A. MATSUNAWA: 'The role of recoil pressure in energy balance during laser materials processing', *Journal of Physics D: Applied Physics*, Vol. 30, No. 18, pp. 2541-2552, 1997.
[17] X. CHEN, H.-X. WANG: 'A calculation model for the evaporation recoil pressure in laser material processing', *Journal of Physics D: Applied Physics*, Vol. 34, No. 17, pp. 2637-2642, 2001.
[18] J. Y. LEE, S. H. KO, D. F. FARSON, C. D. YOO: 'Mechanism of keyhole formation and stability in stationary laser welding', *Journal of Physics D: Applied Physics*, Vol. 35, No. 13, pp. 1570-1576, 2002.